Simulation for Hot Electron Interchange Mode

Zikang Yang,[1] Nanxiang Jiang,[1] Wang Ge,[1] Tianchun Zhou,[2] Bo Li,[1] and M. E. Mauel[3]

[1] *School of Physics, Beihang University, Beijing 100191, China*
[2] *School of Physics, Harbin Institute of Technology, Harbin 150001, China*
[3] *Department of Applied Physics and Applied Mathematics, Columbia University, New York, New York 10027, USA*

(Dated: March 16, 2026)

We present a normalized coordinate formulation for the Hot Electron Interchange (HEI) instability based on experimental parameters from laboratory terrellas [1]. The normalization procedure simplifies the mathematical description while preserving physical accuracy, enabling more efficient numerical simulation of drift-resonant fluctuations and hot electron transport.

I. INTRODUCTION

The Hot Electron Interchange (HEI) instability is a fundamental process in magnetized plasmas confined by a dipole magnetic field, playing a crucial role in the radial transport of energetic particles. This instability has been extensively studied both in the context of planetary magnetospheres and in laboratory experiments, particularly in the Collisionless Terrella Experiment (CTX) [1, 2]. In such configurations, a population of hot electrons trapped in a dipole field can excite low-frequency, flute-like electrostatic fluctuations through drift-resonant wave-particle interactions, leading to cross-field transport and the formation of complex phase-space structures.

Theoretical descriptions of the HEI mode date back to the work of Krall [4], who first identified the instability driven by pressure gradients in a mirror-like geometry. Subsequent analyses extended the theory to dipole geometry, incorporating the effects of finite Larmor radius and ion polarization currents [1]. Experimental observations in CTX have revealed that the instability exhibits a rich nonlinear behavior, including frequency chirping, mode coupling, and the spontaneous formation of phase-space holes and clumps [1, 2]. These phenomena are reminiscent of those predicted by Berk and co-workers for resonant particle instabilities near marginal stability [5, 6].

Despite the progress in understanding the HEI mode, the conventional dimensional formulation of the governing equations involves multiple physical parameters that can obscure the essential scaling relationships and complicate numerical simulations. To address this, we introduce a normalized coordinate framework that simplifies the mathematical description while retaining the full physical content. By scaling the magnetic flux, electrostatic potential, and time with characteristic experimental values from CTX, we derive a set of dimensionless equations that are both computationally efficient and physically transparent.

The primary objectives of this paper are twofold. First, we present a detailed derivation of the normalized equations for the HEI instability, including the hot electron kinetic equation, the ion continuity equation with polarization drift, and the vorticity equation under quasi-neutrality. Second, we employ this normalized formulation to perform nonlinear numerical simulations that investigate the conditions leading to frequency chirping and phase-space structure formation. Our simulations reproduce key experimental features, such as the dependence of the chirping rate on non-resonant dissipation and the role of the particle source in sustaining the nonlinear dynamics. We also explore the energy-dependence of the instability by considering multiple magnetic moment groups and single-μ simulations.

The paper is organized as follows. Section 2 summarizes the classical theory of the HEI mode in dipole geometry, including the magnetic coordinates and basic equations. Section 3 introduces the normalization framework and derives the dimensionless forms of the electron and ion continuity equations, the Poisson equation, and the vorticity equation. Section 4 presents numerical results from our simulations, focusing on the effects of diffusion strength, particle source, and energy distribution on the nonlinear evolution and frequency chirping. Finally, Section 5 concludes with a discussion of the implications and future directions.

II. CLASSICAL THEORY OF HOT ELECTRON INTERCHANGE MODE

The foundational theory for the Hot Electron Interchange (HEI) instability in dipole-confined plasmas was developed based on the Collisionless Terrella Experiment (CTX) [1]. This section summarizes the key elements of that framework, which the present normalized formulation builds upon.

A. Magnetic Coordinates and Basic Equations

In an axisymmetric dipole field, the canonical magnetic coordinates (ψ, φ) are employed, where ψ is the magnetic flux function and φ is the azimuthal angle. In spherical geometry, $\psi = M \sin^2\theta / r$, with $M \equiv B_0 L_0^3$ being the dipole moment.

The model describes a plasma comprising cold ions and a mix of cold and hot (energetic) electrons [1]. The hot

electron population is treated kinetically via a bounce-averaged distribution function $F(\mu, \psi, \varphi, t)$, where μ is the magnetic moment (first adiabatic invariant). The system dynamics are governed by the following coupled equations:

The evolution of hot electron distribution function :

$$\frac{\partial F}{\partial t} + \frac{\partial}{\partial \varphi}\left[(\omega_d + v_\phi)\, F\right] + \frac{\partial}{\partial \psi}\left(v_\psi F\right) = 0, \tag{1}$$

where e is the elementary charge, and B is the magnetic field strength. The magnetic drift frequency for hot electrons is given by [1]

$$\omega_d = \frac{\mu}{e}\frac{\partial B}{\partial \psi} = \frac{3\mu B}{e\psi}. \tag{2}$$

$$v_\phi = -\frac{\partial \Phi}{\partial \psi}, \qquad v_\psi = \frac{\partial \Phi}{\partial \varphi}. \tag{3}$$

Continuity equation for cold ions (including polarization drift) [1]:

$$\frac{\partial N_i}{\partial t} + \frac{\partial}{\partial \varphi}\left(N_i v_\phi\right) + \frac{\partial}{\partial \psi}\left(N_i v_\psi\right) - \frac{\partial}{\partial \varphi}\left(N_{i0}\cdot 0.66\frac{M^2 B_0}{\psi^4 \omega_{ci0}}\frac{\partial^2 \Phi}{\partial \varphi \partial t}\right) - \frac{\partial}{\partial \psi}\left(N_{i0}\cdot 0.77\frac{M^2 B_0}{\psi^2 \omega_{ci0}}\frac{\partial^2 \Phi}{\partial \psi \partial t}\right) = 0, \tag{4}$$

where $\omega_{ci0} = eB_0/M_i$ is the reference ion cyclotron frequency (with M_i the ion mass).

Field-line averaged Poisson's equation [1]:

$$\frac{\partial}{\partial \varphi}\left(2\frac{M}{\psi^2}\frac{\partial \Phi}{\partial \varphi}\right) + \frac{\partial}{\partial \psi}\left(4M\frac{\partial \Phi}{\partial \psi}\right) = -4\pi e\left(N_i - N_e\right), \tag{5}$$

where Φ is the electrostatic potential, N_i and $N_e = \int F\, d\mu$ are particle number of electrons and ions per unit flux.

III. NORMALIZATION FRAMEWORK

A. Dimensionless Coordinates

We introduce normalized magnetic coordinates based on characteristic experimental values from CTX [1]:

$$x \equiv \frac{\psi}{\psi_0}, \quad y \equiv \varphi \tag{6}$$

where $\psi_0 = B_0 L_0^2$ is the reference magnetic flux, with $B_0 = 875\,\mathrm{G}$ and $L_0 = 27\,\mathrm{cm}$ [1].

The electrostatic potential is normalized to:

$$\phi \to \frac{3\mu_0 B_0}{e} \tag{7}$$

where $\mu_0 = 9 \times 10^{-12}\,\mathrm{erg/G}$ is the reference magnetic moment for hot electrons, based on CTX experimental parameters [1].

B. Normalized Time

We introduce a normalized time variable:

$$\tau = \omega_{d0} t, \tag{8}$$

where ω_{d0} is the characteristic magnetic drift frequency for hot electrons [1], defined as

$$\omega_{d0} = \frac{3\mu_0 B_0}{e\psi_0}. \tag{9}$$

This normalization ensures that the time evolution is scaled by the characteristic drift period of hot electrons observed in CTX [1].

C. Normalized Distribution Function and Density

We define the normalized distribution function and densities with explicit dependence on the magnetic flux:

$$F(x, y, \tau, \mu) \equiv \frac{F(\psi, \varphi, t, \mu)}{F_0(\psi_0)}, \tag{10}$$

$$\hat{N}_i(x, y, \tau) \equiv \frac{N_i(\psi, \varphi, t)}{N_{i0}(\psi_0)}, \tag{11}$$

$$\hat{N}_h(x, y, \tau) \equiv \frac{N_h(\psi, \varphi, t)}{N_{i0}(\psi_0)}, \tag{12}$$

$$\hat{N}_c(x, y, \tau) \equiv \frac{N_c(\psi, \varphi, t)}{N_{i0}(\psi_0)}, \tag{13}$$

where $F_0(\psi_0)$ is the reference distribution function and $N_0 \equiv N_{i0}(\psi_0)$ is the reference ion density, both evaluated at the reference flux surface $\psi = \psi_0$ (i.e., $x = 1$).

The normalized total electron density is then $\hat{N}_e = \hat{N}_c + \hat{N}_h$.

D. Hot Electron Distribution Evolution

Applying our normalization framework to Eq. (1), we obtain that evolution of hot electron distribution function is governed by:

$$\frac{\partial F}{\partial t} + \frac{\partial}{\partial y}\left[(\hat{\omega}_d + v_y)F\right] + \frac{\partial}{\partial x}(v_x F) = S, \tag{14}$$

where S represents the particle source term and the

normalized variables are:

$$\hat{\omega}_d = \frac{\omega_d}{\omega_{d0}} = \hat{\mu}x^2, \quad \hat{\mu} = \frac{\mu}{\mu_0} \tag{15}$$

$$v_y = -\frac{\partial\phi}{\partial x}, \quad v_x = \frac{\partial\phi}{\partial y} \tag{16}$$

The characteristic drift frequency is $\omega_{d0} = 2\pi \times 0.4\,\text{Mrad/s}$ for hot electrons in CTX [1].

E. Derivation of Electron Continuity Equation

The total electron continuity equation is derived by combining the contributions from both cold and hot electrons [1]. The hot electron distribution evolves according to equation (10). Integrating equation (10) over the magnetic moment μ yields the continuity equation for hot electrons alone. The cold electrons, which are not subject to magnetic drifts, obey a simpler continuity equation with only $\mathbf{E}\times\mathbf{B}$ convection [1].

a. Hot electron continuity. Define the hot electron density as

$$N_h(x,y,t) = \int d\mu\, F(x,y,t,\mu). \tag{17}$$

Integrating equation (10) over μ and interchanging integration and differentiation gives

$$\frac{\partial}{\partial t}N_h + \frac{\partial}{\partial y}\left(v_y N_h + \int d\mu\, \hat{\omega}_d F\right) + \frac{\partial}{\partial x}\left(v_x N_h\right) = 0. \tag{18}$$

The term $\int d\mu\, \hat{\omega}_d F_\mu$ represents the additional toroidal drift current carried by hot electrons [1].

b. Cold electron continuity. Cold electrons are assumed to follow only $\mathbf{E}\times\mathbf{B}$ convection, so their density N_c satisfies [1]

$$\frac{\partial}{\partial t}N_c + \frac{\partial}{\partial y}(v_y N_c) + \frac{\partial}{\partial x}(v_x N_c) = 0. \tag{19}$$

c. Total electron continuity. The total electron density is $N_e = N_c + N_h$ [1]. Adding equations (18) and (19) gives

$$\dot{N}_e + \frac{\partial}{\partial y}(v_y N_e) + \frac{\partial}{\partial x}(v_x N_e) + \frac{\partial}{\partial y}\int \mathrm{d}\mu\, \hat{\omega}_d(\mu) F = 0 \tag{20}$$

which is the total electron continuity equation [1]. This derivation highlights that the hot electrons contribute an extra toroidal drift term, while the cold electrons contribute only the common $\mathbf{E}\times\mathbf{B}$ convection terms.

F. Ion Continuity Equation with Polarization Drifts

The cold ion evolution includes polarization drift effects [1]:

$$\dot{N}_i + \frac{\partial}{\partial y}(v_y N_i) + \frac{\partial}{\partial x}(v_x N_i) - \frac{\omega_{d0}}{\omega_{ci0}}\left(\frac{\partial}{\partial y}N_i u_y + \frac{\partial}{\partial x}N_i u_x\right) = 0 \tag{21}$$

This is the new normalized form of Eq. (4). with polarization drift components [1]:

$$u_y = \frac{0.6}{x^4}\frac{\partial}{\partial y}\dot{\phi} \tag{22}$$

$$u_x = \frac{0.7}{x^2}\frac{\partial}{\partial x}\dot{\phi} \tag{23}$$

Under the assumption of slowly varying density, $N_i \approx N_0 = 1$,the polarization divergence simplifies to [1]:

$$\frac{\partial}{\partial y}(N_i u_y) + \frac{\partial}{\partial x}(N_i u_x) \simeq N_0\frac{\partial u_y}{\partial y} + N_0\frac{\partial u_x}{\partial x} \simeq \frac{0.6}{x^4}\frac{\partial^2}{\partial y^2}\dot{\phi} + \frac{0.7}{x^2}\frac{\partial^2}{\partial x^2}\dot{\phi} \tag{24}$$

G. Poisson Equation and Quasi-Neutrality

The normalized Poisson equation in dipole coordinates [1]:

$$\frac{2}{x^2}\frac{\partial^2}{\partial y^2}\dot{\phi} + 4\frac{\partial^2}{\partial x^2}\dot{\phi} = 0.91\left(\frac{L_0}{\lambda_D}\right)^2(\dot{N}_e - \dot{N}_i) \tag{25}$$

This is the new normalized form of Eq. (5). Given the experimental parameter from CTX [1]:

$$\left(\frac{L_0}{\lambda_D}\right)^2 \approx 10^3 \gg 1 \tag{26}$$

the right-hand side dominates, enforcing quasi-neutrality [1]:

$$N_e = N_i \tag{27}$$

$$\dot{N}_e - \dot{N}_i = 0 \tag{28}$$

H. Vorticity Equation

To derive the vorticity equation, we use the ion continuity equation (21) , along with the electron continuity equation (20) and the quasi-neutrality condition (28) [1]. This yields:

$$\frac{\partial}{\partial y}\int \mathrm{d}\mu\, \hat{\omega}_d F + \frac{N_{i0}}{\hat{\omega}_{ci0}}\left(\frac{0.6}{x^4}\frac{\partial^2}{\partial y^2} + \frac{0.7}{x^2}\frac{\partial^2}{\partial x^2}\right)\dot{\phi} = 0 \tag{29}$$

with the experimental frequency ratio from CTX: $\hat{\omega}_{ci0} = \omega_{ci0}/\omega_{d0} = 3.5$ [1]. This vorticity equation couples the

hot electron drift resonance with the cold ion polarization drift, providing a complete description of the HEI dynamics in normalized coordinates [1].

I. Linear Instability Analysis

1. Perturbed hot-electron distribution

According to the linearized kinetic equation (10), the perturbed hot electron distribution function can be expressed as [1]:

$$\tilde{F} = \frac{m\tilde{\phi}}{\omega - m\omega_d}\frac{\partial F_0}{\partial x} \tag{30}$$

where m is the azimuthal mode number, ω is the complex frequency, and F_0 is the equilibrium distribution function.

2. Equilibrium distribution function

Under our normalization conditions, we consider only the hot electron component [1]:

$$F_0 = N_{i0}\alpha G(\mu)\delta(J) \tag{31}$$

where $\alpha \equiv N_h/N_i$ is the fraction of hot electrons relative to the total ion density, $G(\mu)$ is the normalized distribution function in magnetic moment satisfying $\int G(\mu)\, d\mu = 1$, and $\delta(J)$ indicates that electrons are deeply trapped in the equatorial plane ($J = 0$).

3. Fourier transformed vorticity equation

Under the approximation that the instability is localized near the reference magnetic surface ($x \approx 1$),by performing Fourier transform on equation (29), we obtain [1]:

$$im\int d\mu\, \hat{\omega}_d F + \frac{N_{i0}}{\hat{\omega}_{ci0}}\left(0.6(-m^2) + 0.7(-k_x^2)\right)(-i\omega\phi) = 0 \tag{32}$$

For the regime where the azimuthal mode number dominates the radial structure ($m \gg k_x$), the k_x^2 term can be neglected. This simplifies the equation to [1]:

$$m\int d\mu\, \hat{\omega}_d F + \frac{0.6}{\hat{\omega}_{ci0}} N_{i0} m^2 \omega\phi = 0 \tag{33}$$

4. Dispersion relation

Substituting equations (30) and (31) into equation (33), we obtain [1]:

$$m^2\frac{\partial(N_{i0}\alpha)}{\partial x}\int d\mu \frac{\omega_d G(\mu)}{\omega - m\omega_d}\phi + \frac{0.6}{\hat{\omega}_{ci0}} N_{i0} m^2 \omega\phi = 0 \tag{34}$$

Setting $G(\mu) = \delta(\mu - \mu_0)$, and noting that $\omega_d(\mu_0) = \hat{\mu}x^2$with $\hat{\mu} = 1$, we obtain the following dispersion relation [1]:

$$\frac{\partial(N_{i0}\alpha)}{\partial x}\frac{\omega_d(\mu_0)}{\omega - m\omega_d(\mu_0)} + \frac{0.6}{\hat{\omega}_{ci0}} N_{i0}\omega = 0 \tag{35}$$

Under the typical experimental condition where modes are localized near the reference flux surface ($x \approx 1$) and noting that the second term is small for the parameters of interest, we obtain the simplified dispersion relation [1]:

$$\omega^2 - m\omega_d(\mu_0)\omega + \Gamma_h^2 = 0 \tag{36}$$

where we define the hot electron interchange drive strength Γ_h^2 as [1]:

$$\Gamma_h^2 \equiv \frac{1.5}{N_{i0}}\hat{\omega}_{ci0}\omega_d(\mu_0)\frac{\partial(N_{i0}\alpha)}{\partial x} \tag{37}$$

5. Frequency and growth rate

Solving the quadratic equation (36) for the complex frequency ω yields [1]:

$$\omega = \frac{m\omega_d(\mu_0)}{2} \pm \frac{1}{2}\sqrt{m^2\omega_{d0}^2 - 4\Gamma_h^2} \tag{38}$$

The corresponding instability growth rate $\gamma = \mathrm{Im}(\omega)$ is [1]:

$$\gamma = \frac{1}{2}\sqrt{4\Gamma_h^2 - m^2\omega_d^2(\mu_0)} \tag{39}$$

This result clearly shows that the instability is driven by the hot electron gradient (through Γ_h^2), while stability is determined by the hot electron drift frequency (ω_{d0}) [1]. The instability condition is $\Gamma_h^2 > (m^2/4)\omega_{d0}^2$ [1].

IV. NUMERICAL INVESTIGATION OF NONLINEAR DYNAMICS AND FREQUENCY CHIRPING

Building upon the normalized framework established in previous sections, we have conducted a series of numerical simulations to investigate the nonlinear evolution of the HEI instability, with a particular focus on the conditions leading to frequency chirping and the formation

of phase-space structures. This section presents the key findings from these recent numerical experiments.

All simulations presented herein were performed on a domain $x \in [0.3, 1.5]$, $y \in [0, 2\pi]$ with a 128×128 grid. The hot electron population is modeled with four discrete magnetic moment values, $\mu = [0.5, 0.75, 1.0, 1.25]$, and an energy distribution shape parameter of $l = 2$ as per Eq. (18) in [1]. An initial hot-electron density profile with a peak amplitude of amp $= 0.2$ is imposed. A particle source with amplitude source_amplitude $= 0.005$ is present to sustain the hot electron population, unless otherwise stated. To ensure numerical stability and to model the non-resonant dissipation present in the experiment [1], we explicitly introduce an artificial diffusion term in the time advancement of the electrostatic potential ϕ. The potential update adopts a form consistent with Eq. (19) of [1]. For the second-order diffusion considered in this work (i.e., taking $k = 1$ in Eq. (19)), the sign factor in front of the diffusion term becomes $-(-1)^k = +1$, leading to the specific update scheme:

$$\phi(t + \Delta t) = \phi(t) + \Delta t\, \dot{\phi} + \nu \Delta t\, \nabla^2 \phi(t), \qquad (40)$$

where ν is the diffusion coefficient (corresponding to ν in Ref. [1] and the variable `dif` in the code), and ∇^2 is the two-dimensional Laplacian operator. The positive sign ensures damping of high-frequency modes.

A. Effect of Diffusion Strength on Nonlinear Evolution

We first examine the effect of varying the diffusion coefficient ν. Three cases were simulated: '$\nu = 0.001$', '$\nu = 0.002$', and '$\nu = 0.004$', with all other parameters held constant.

In the '$\nu = 0.001$' case, the simulation successfully reproduces key nonlinear phenomena described by Mauel [1]. As shown in Fig. 1, we observe the formation of coherent phase-space "holes"—localized depletions in the hot electron distribution function $F_\mu(x, y)$. The instability exhibits a clear energy-dependent behavior, exciting lower-energy ($\mu = 0.5$) electrons first, followed by higher-energy populations. The phase-space structures for $\mu = 0.5$ appear more turbulent, while those at higher μ values are more coherent and stable. Concurrent with the formation of these structures, a distinct frequency chirping (upsweeping) is observed, with the dominant frequency increasing from an initial value of ~ 0.5 to ~ 1.0 over the simulation runtime of 20,000 steps.

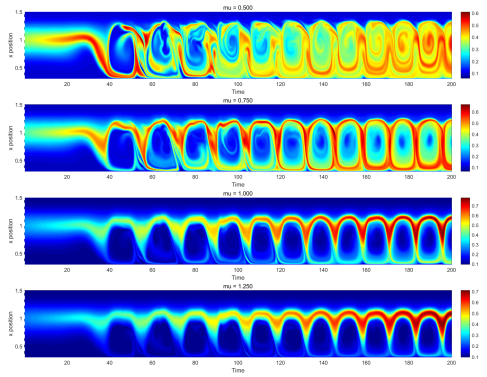

FIG. 1: Phase-space structures ($F_\mu(x, y)$) observed in the 'ν=0.001' simulation, showing coherent "holes" at higher μ values and more turbulent structures at $\mu = 0.5$.

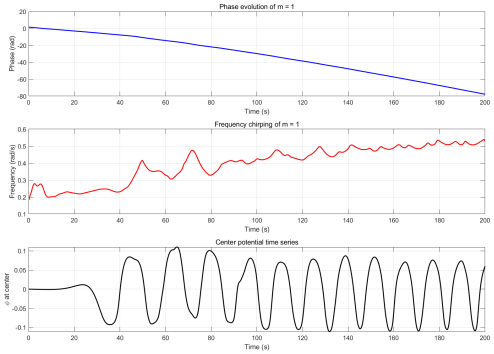

FIG. 2: Time evolution for the 'ν=0.001' case: (a) phase of $m = 1$ mode, (b) instantaneous frequency (chirping), and (c) electrostatic potential at the plasma center.

1. *The Baseline Case: $\nu = 0.002$*

Increasing the diffusion to '$\nu = 0.002$' leads to a more pronounced frequency chirping. To illustrate the evolution concretely, we present in Figs. 3 and 4 snapshots of the electrostatic potential and phase-space distribution at two characteristic times for this case.

The frequency chirping accompanying this evolution is shown in Fig. 5. The dominant frequency sweeps from ~ 0.5 to ~ 1.4 over the same period, aligning well with observations in related studies that link increased dissipation to more effective frequency sweeping [1]. The overall morphology of the phase-space holes remains similar to the 'ν=0.001' case. However, a notable effect is a reduction in the peak amplitude of the fluctuations, consistent with enhanced dissipation damping the wave growth. Given the clearer chirping signal, we select '$\nu = 0.002$' as the baseline parameter for subsequent studies.

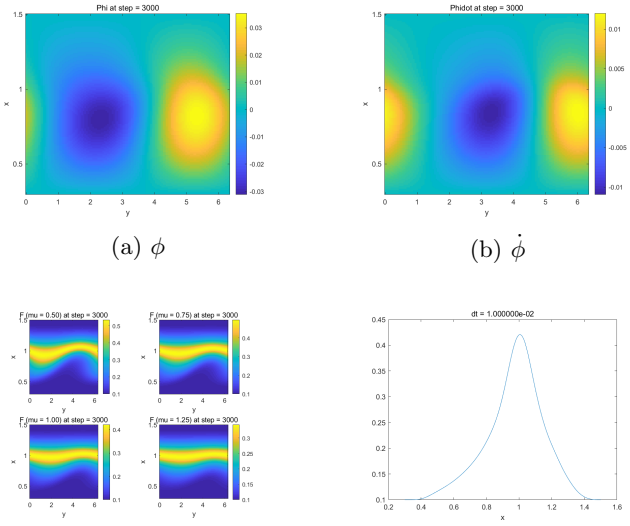

(a) ϕ (b) $\dot{\phi}$

(c) $F_{\mu=1.0}(x, y)$ (d) $F_{\mu=1.0}(x)$ at $y = \pi$

FIG. 3: Linear growth stage ($t \approx 30$). The potential exhibits a regular $m = 1$ pattern, and the phase-space distribution shows periodic modulations but no coherent holes yet.

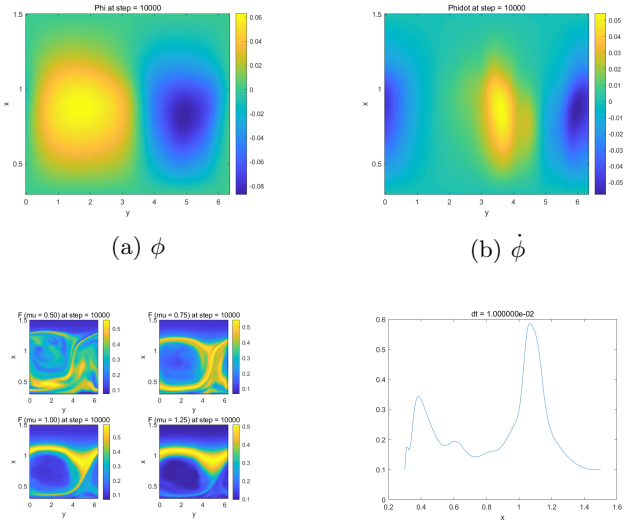

(a) ϕ (b) $\dot{\phi}$

(c) $F_{\mu=1.0}(x, y)$ (d) $F_{\mu=1.0}(x)$ at $y = \pi$

FIG. 4: Nonlinear stage ($t \approx 150$). The potential develops localized structures, and clear phase-space "holes" (depressions in F_μ) are visible, which propagate inward and are responsible for the frequency chirping.

2. *Quantitative Analysis of the Baseline Case (ν=0.002)*

For the baseline case with '$\nu = 0.002$', we have extracted quantitative characteristics of both the linear and nonlinear stages. During the linear phase (approximately $t < 40$), the dominant $m = 1$ mode oscillates with a real frequency $\omega_r \approx 0.22$–0.25 (normalized to

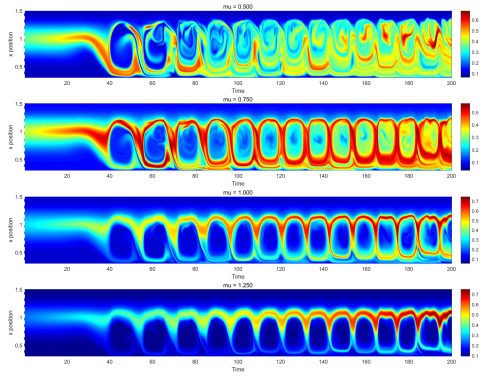

FIG. 5: Frequency chirping observed in the 'ν=0.002' simulation. The dominant frequency shows a clear upsweep from ~ 0.5 to ~ 1.4 over the simulation period.

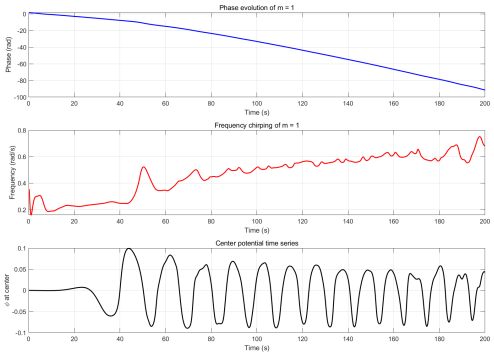

FIG. 6: Time evolution for the 'ν=0.002' baseline case.

ω_{d0}), which agrees well with the theoretical prediction $\omega_r = m\omega_d/2 \approx 0.25$ from Eq. (38) for $m = 1$ and resonance position$x \approx 0.8$ at the reference flux surface. The exponential growth of the mode amplitude yields a linear growth rate $\gamma \approx 0.15$ (normalized).

In the nonlinear saturated regime, a clear frequency upsweep is observed. The instantaneous frequency of the $m = 1$ mode increases from ~ 0.3 to ~ 0.7 over the simulation period. To quantify the chirping strength, we compute the normalized frequency chirping rate $\dot{\omega}/\omega^2$, which is the standard measure used in experimental studies [1]. Averaging over the nonlinear stage (from $t = 50$ to $t = 200$) gives $\frac{\dot{\omega}}{\omega^2} = 0.0102$ This value lies between the two experimental regimes reported in CTX: the rapid chirping during heating bursts ($\dot{\omega}/\omega^2 \sim 0.2$) and the much slower chirping in the afterglow ($\dot{\omega}/\omega^2 \sim 2 \times 10^{-4}$) [1]. Our simulated normalized chirping rate 0.01 is also smaller than the values 0.07 and 0.2 mentioned in Mauel's paper [1].The intermediate value obtained in our simulation is consistent with the moderate dissipation level ('ν=0.002') used, and confirms that non-resonant diffusion controls the rate of frequency sweeping, as predicted by Berk et al. [1] and observed in the numerical experi-

ments of Mauel [1].

These quantitative results demonstrate that our normalized simulation faithfully reproduces both the linear dispersion relation and the key nonlinear scaling laws of the HEI instability.

A further increase of the diffusion to '$\nu = 0.004$' results in a dramatic suppression of the instability. As illustrated in Fig. 7, the fluctuation amplitude decays significantly over time, approaching zero by the end of the simulation. While frequency chirping is still present, ranging from ~ 0.5 to ~ 0.8, the weak amplitude makes the signal less coherent. In this highly dissipative regime, the phase-space structures begin to break down; significant turbulence is observed not only for $\mu = 0.5$ but also begins for $\mu = 0.75$, whose hole structure deforms towards the end of the simulation. Only the highest energy populations ($\mu = 1.0$ and 1.25) retain relatively coherent structures.

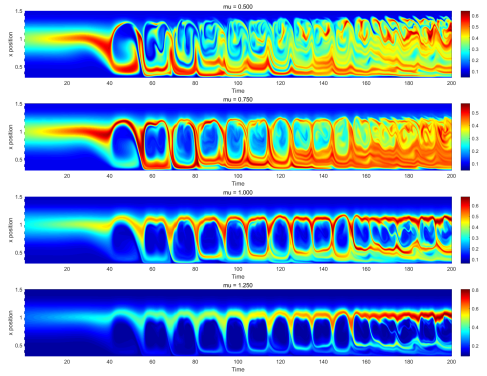

FIG. 7: Amplitude decay and phase-space structure deformation in the highly dissipative 'ν=0.004' simulation. The fluctuation amplitude is significantly reduced.

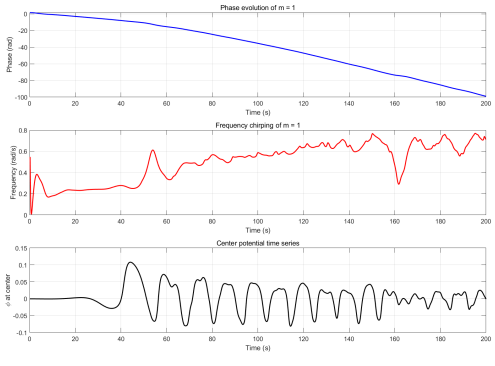

FIG. 8: Time evolution for the highly dissipative 'dif=0.004' case.

B. Role of the Particle Source in Sustaining Nonlinear Dynamics

To isolate the role of the hot electron source, we performed a simulation with '$\nu = 0.002$' but with the source term removed (source_amplitude = 0.0). This configuration closely mirrors the simulation setup discussed by Mauel [1]. The results, shown in Fig. 9, exhibit several key differences from the baseline with a source.

First, the inward radial propagation of phase-space holes is exceptionally clear. Second, the absence of a source leads to a natural decay of the instability as free energy is extracted. The maximum fluctuation amplitude decreases from ~ 0.7 to ~ 0.2 over the simulation, a more rapid decay compared to the source-driven case where amplitude dropped from ~ 1.0 to ~ 0.4. Consequently, the total frequency chirp is reduced, reaching a final value of ~ 1.0 compared to ~ 1.4 in the source-present case. This suggests that the particle source provides a continuous supply of free energy, allowing the nonlinear evolution and frequency sweeping to proceed to a greater extent.

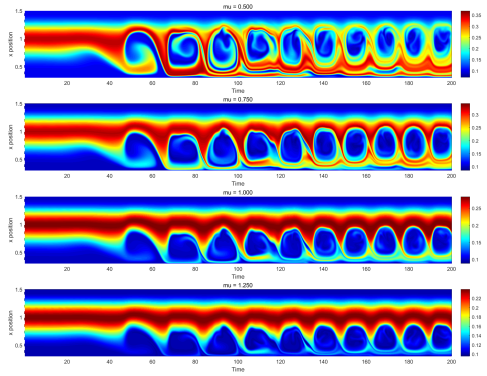

FIG. 9: Phase-space evolution in the absence of a particle source. Clear inward propagation of holes and amplitude decay are observed.

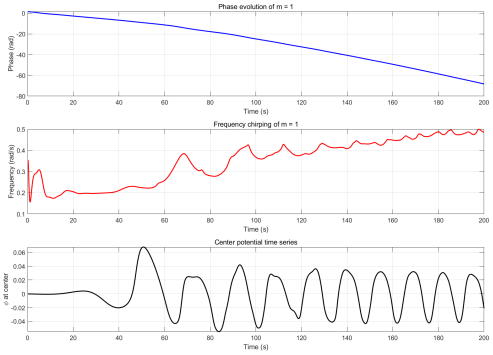

FIG. 10: Time evolution without particle source, showing clear inward propagation of holes and amplitude decay.

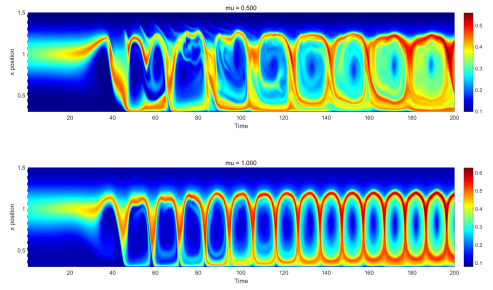

FIG. 11: Comparison of frequency chirping in single-μ simulations. Both $\mu = 0.5$ and $\mu = 1.0$ show chirping, with the higher energy case exhibiting a much stronger effect.

C. Energy-Dependence of Frequency Chirping: Single-μ Simulations

To investigate which energy population predominantly drives the frequency chirping, we conducted two simulations using the baseline 'ν=0.002' parameters but with only a single magnetic moment value: one with $\mu = 0.5$ (lower energy) and one with $\mu = 1.0$ (higher energy). The results, summarized in Fig. 11, challenge our initial hypothesis.

Contrary to the expectation that low-energy electrons initiate the chirp and high-energy electrons sustain it later, both single-μ simulations exhibited frequency chirping independently. Furthermore, the chirp onset time, or the "knee" in the frequency evolution curve, is nearly identical for both cases. Notably, the higher-energy ($\mu = 1.0$) simulation produced a much stronger frequency sweep, rising to a final value comparable to the full multi-μ case. This indicates that while low-energy electrons contribute to the initial perturbation and turbulence, the high-energy population is capable of independently generating and sustaining a strong frequency chirp through its resonant interaction with the wave. The dynamics are more complex than a simple sequential activation model.

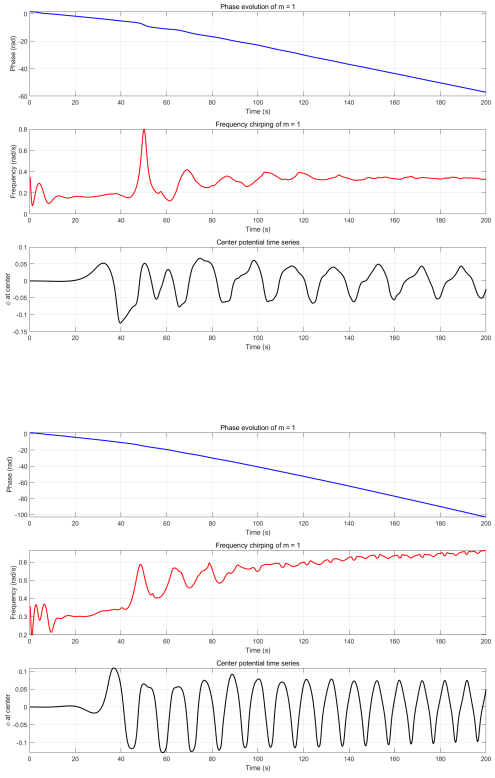

FIG. 12: Time evolution for single-μ simulations: top $\mu = 0.5$, bottom $\mu = 1.0$.

D. Effect of Multimode Initial Perturbation

To explore the influence of initial azimuthal mode spectrum on the nonlinear evolution, we performed a simulation with the same baseline parameters (‘ν=0.002‘, source on) but initialized the electrostatic potential with a superposition of multiple azimuthal modes. Specifically, the initial perturbation was generated using ‘addRandomSin2D‘ with the last two arguments set to ‘10, 10‘, meaning that 10 random modes in the y-direction were excited, as opposed to the single-mode (‘10, 1‘) initialization used in previous cases.

The results are summarized in Fig. 13.

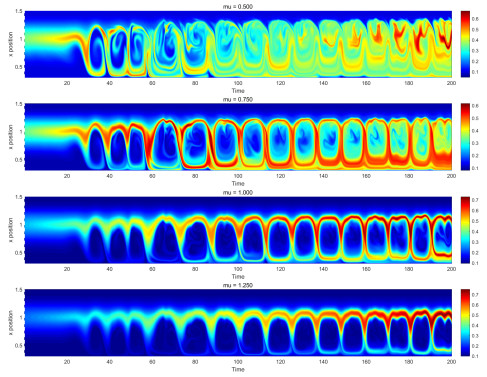

FIG. 13: Time evolution for the multimode initial perturbation case.

V. CONCLUSION

We have implemented a normalized coordinate framework for the Hot Electron Interchange instability based on experimental parameters from laboratory terrellas [1]. The formulation simplifies numerical implementation while maintaining physical accuracy, providing a solid foundation for efficient simulation of drift-resonant fluctuations and hot electron transport.

The key achievement is the derivation of a single vorticity equation that encapsulates the essential physics while being computationally tractable [1]. This work enables more systematic parameter studies and clearer physical interpretation of simulation results. Our recent numerical experiments have successfully reproduced key nonlinear phenomena such as phase-space hole formation and frequency chirping. We have demonstrated that the strength of non-resonant diffusion (ν) critically controls the chirping range and amplitude, with an optimal value (‘ν=0.002‘) yielding the most pronounced effect. The presence of a particle source sustains the instability, allowing for a wider frequency sweep. Finally, single-μ simulations reveal that high-energy electrons alone are sufficient to drive strong frequency chirping, providing new insight into the nonlinear dynamics of the HEI mode.

[1] Mauel, M. E. (1997). Laboratory Observations of Wave-Induced Radial Transport within an “Artificial Radiation Belt”. *J. Phys. IV France*, 7, C4-307-C4-318.

[2] B. Levitt, D. Maslovsky, and M. E. Mauel, “Measurement of the global structure of interchange modes driven by energetic electrons trapped in a magnetic dipole,” *Phys. Plasmas*, 9, 2507 (2002).

[3] E. E. Ortiz, A. C. Boxer, J. L. Ellsworth, D. T. Garnier, A. K. Hansen, I. Karim, J. Kesner, and M. E. Mauel, “Effects of the Hot Electron Interchange Instability on Plasma Confined in a Dipolar Magnetic Field,” *J. Fusion Energy*, 26, 139 (2007).

[4] N. A. Krall, “Stabilization of Hot Electron Plasma by a Cold Background,” *Phys. Fluids*, 9, 820 (1966).

[5] Berk, H. L., et al., Phys. Plasmas 4, 1075 (1997).

[6] Berk, H. L., et al., Phys. Plasmas 6, 3102 (1999).